In Situ Scanning Tunneling Microscopy of Corrosion of Silver-Gold Alloys

Ivette C. Oppenheim, Dennis J. Trevor,
Christopher E. D. Chidsey,* Paula L. Trevor, Karl Sieradzki*

An in situ scanning tunneling microscope (STM) was used to observe the morphological changes accompanying the selective dissolution of Ag from low-Ag content Ag-Au alloys in dilute perchloric acid. This study was undertaken to explore the role of surface diffusion in alloy corrosion processes. These results are interpreted within the framework of the kink-ledge-terrace model of a crystal surface and a recent model of alloy corrosion based on a variant of percolation theory. The corrosion process leads to roughening of the surface by dissolution of Ag atoms from terrace sites. Annealing or smoothening of the surface occurs by vacancy migration through clusters and the subsequent annihilation of clusters at terrace ledges.

De-alloying, the selective dissolution of one or more of the elements of an alloy owing to large differences in their reactivities, is important in the passivation (*1*), pitting (*2*), and stress-corrosion cracking (*3*) of technologically significant metals, such as stainless steel and the lightweight Al-Li alloys currently under development. Various mechanisms of de-alloying have been proposed (*4–6*), but a full understanding of this important process is still an open issue. Sieradzki *et al.* (*6*) have recently proposed a model of selective dissolution for a binary alloy based on a variant of percolation theory that allows for the removal of one element while the other undergoes surface diffusion. In general, rearrangement of the surface by diffusion of the less reactive element can result in the covering or uncovering of underlying atoms of the more reactive element. Sieradzki *et al.* (*6*) suggested that this kinetic coupling of dissolution and diffusion results in a composition-dependent "critical potential" below which bulk de-alloying does not occur, even for alloys with concentrations of the more reactive element above the three-dimensional (3-D) percolation threshold. The need for an atomic-level understanding of both the dissolution and diffusion components of the de-alloying process has motivated the STM study reported here.

We used the in situ STM technique (*7–15*) to study the changes in surface morphology accompanying the selective dissolution of Ag from Ag-Au alloys in contact with 0.1 M $HClO_4$. The Ag-Au system was chosen for the experimental convenience of having air-stable surfaces. Alloys with Ag concentrations well below the site percolation threshold were used to limit the Ag dissolution to the first few atomic layers so that the STM could faithfully follow the surface morphology. Our results on the evolution of the surface morphology at the atomic level provide a microscopic basis for modeling the role of dissolution and surface diffusion in corrosion.

Ag-Au alloy films with exclusively {111} texture were prepared by simultaneous vapor deposition of Ag and Au onto heated mica substrates (*16*). The bulk sample compositions were obtained by energy dispersive x-ray fluorescence analysis (*17*). Samples were mounted in a modified Nanoscope I STM (Digital Instruments) that allows for imaging in an electrolyte solution with control of the electrochemical potentials of both the sample and the tunneling tip (*9, 10*). All electrochemical potentials are reported with respect to a Ag/(1 mM $AgClO_4$, 0.1 M $HClO_4$) reference electrode. The $Pt_{0.8}Ir_{0.2}$ tunneling tips were electrochemically etched to a point and coated with an insulator on all but the very end to minimize electrochemical currents (*9, 10*). The lateral resolution of these tips is typically about 2 nm wide, as measured by the observed width of monatomic ledges on Au (111). The STM was operated in the constant-current mode with a tunneling current of 1 nA (*18*) and a tip bias of −0.01 to −0.53 V with respect to the sample, depending on the electrochemical potential of the sample. The 200 nm by 200 nm images presented here were obtained at a rate of 400 nm/s, which corresponds to an acquisition time of 2 min per image.

Figure 1 shows a time sequence of four images of a $Ag_{0.07}Au_{0.93}$ alloy after the electrochemical potential was scanned at a rate of 0.02 V/s from the open circuit potential (+0.08 V) to +0.60 V in order to initiate dissolution of Ag from the alloy surface. The electrochemical current density recorded during this scan is shown in the inset to Fig. 1A. The area under the peak in the inset (40 μC/cm²) corresponds to 20% of the charge required to dissolve a monolayer of Ag (111); however, this may be an underestimate of the total change as the electrochemical current did not drop to zero immediately after reaching +0.60 V. The sample surface is composed of flat terrace regions separated by ledges of monatomic height and is similar to vicinal (111) surfaces of Au observed in vacuum (*19*), air (*20*), and electrolytes (*8, 9*). Figure 1A shows the surface morphology observed within 2 min of scanning the potential to +0.60 V. The image is similar to that observed at the open circuit potential (*21*), despite the significant electrochemical charge recorded in the interim, indicating that any change in the surface structure that may have occurred up to this stage is below the lateral resolution of the tip. Images acquired subsequent to Fig. 1A show the surface becoming noticeably rough, and Fig. 1B, taken 10 min after reaching +0.60 V, shows substantial roughening. The roughened crystal planes evolved into monolayer-deep pits or vacancy clusters as large as 16 nm in diameter (Fig. 1C). Pits near the ledges eventually fused with them and left the ledges highly curved (Fig. 1D).

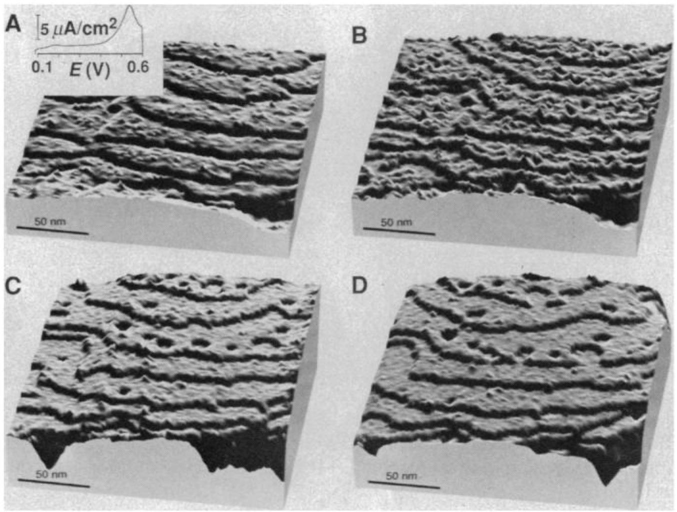

Fig. 1. A time sequence of in situ STM images of the corrosion of a $Ag_{0.07}Au_{0.93}$ alloy sample in 0.1 M $HClO_4$ (**A**) immediately, (**B**) 10 min, (**C**) 51 min, and (**D**) 86 min after scanning the electrochemical potential of the sample to +0.60 V. Vertical scale ×10. Inset shows the electrochemical current density recorded during the 0.02 V/s potential scan.

I. C. Oppenheim and K. Sieradzki, Department of Materials Science and Engineering, The Johns Hopkins University, Baltimore, MD 21218.
D. J. Trevor, C. E. D. Chidsey, P. L. Trevor, AT&T Bell Laboratories, 600 Mountain Avenue, Murray Hill, NJ 07974.

*To whom correspondence should be addressed.

Similar experiments were performed on alloys with lower ($Ag_{0.04}Au_{0.96}$, Fig. 2) and higher ($Ag_{0.15}Au_{0.85}$, Fig. 3) Ag contents (*22*). Effects similar to those discussed above are seen. In the case of the more dilute alloy, roughening was barely noticeable after 10 min at +0.60 V (Fig. 2B) but was observed immediately at +0.70 V (Fig. 2C). In this case mostly small clusters, less than 4 nm in diameter, developed. The terraces also shrank in extent. The grain boundary running horizontally in Fig. 2 serves as a convenient fiducial marker that allows us to measure a ledge recession of order 12 nm in the 120-s interval between acquisition of the image in Fig. 2C and acquisition of the next image. A time series of STM micrographs (Fig. 3) shows how terraces actually break up into smaller terraces in the higher Ag content alloy (*23*). The extent of roughening in this alloy is significantly greater than that observed in the alloys containing less Ag, and the higher Ag content results in a larger overall change in surface morphology.

The surface roughening and subsequent surface rearrangement in the sequences of images presented here are qualitatively similar to the roughening and annealing seen after oxidation and re-reduction of Au (111) (*9*). However, despite the similarity, the two sets of phenomena have quite different origins. The effects seen here require Ag in the sample; pure Au films are unaffected by the electrochemical potentials used here.

There is a substantial (~0.5 V) increase in the formal potential for Ag dissolution from these alloys as compared to the potential for dissolution from pure Ag (*24*). This stabilization is similar to that observed for stripping an underpotentially deposited (UPD) "monolayer" of Ag from Au (111) and reflects the significant additional bond strength that a Ag atom has when bound to Au atoms as compared to other Ag atoms.

Selective dissolution processes in alloys can be interpreted within the framework of the kink-step-terrace model of a crystal surface and percolation theory. In a Ag-dilute Ag-Au alloy, the availability of Ag atoms at ledges is quickly exhausted, and dissolution can only proceed if the electrochemical overpotential is sufficient to remove Ag atoms from terrace sites in the crystal surface. The sequences of images shown in Figs. 1 and 2 clearly indicate the appearance of monatomic deep pits in the terraces of the dealloyed crystal surface, providing strong evidence that Ag atoms are being removed from terrace sites during the dissolution process. In principle, selective removal of Ag from the bulk of the alloy is possible only if the Ag concentration is above the 3-D site percolation threshold. For alloys at compositions below that at which Ag atoms percolate, dissolution from terrace sites occurs until the accessible Ag atoms are exhausted. The resultant (roughened) Au surface rearranges by a vacancy diffusion mechanism. Figures 1 and 2 illustrate this point, showing that the annealing of the surface occurs by concomitant vacancy cluster growth and vacancy cluster annihilation at terrace ledges, the driving force for which is the overall reduction of the surface free energy.

As the Ag concentration in the alloy increases, the connectivity and size of the vacancy clusters that are "injected" into the surface by dissolution increase. Near the two-dimensional (2-D) site percolation threshold, this trend would cause the initial terraces to break up into smaller, more numerous terraces. This behavior is observed for the $Ag_{0.15}Au_{0.85}$ alloy (Fig. 3). From the known degree of surface segregation in Ag-Au alloys (*25*), we estimate the surface composition to be $Ag_{0.36}Au_{0.64}$, which is significantly above the 2-D site percolation threshold of 0.29 for the triangular lattice (*26*).

Our in situ STM results indicate that it takes many minutes at +0.60 V before the surface appears rough at the resolution of our STM (vacancy cluster diameter, ≥2 nm). We offer two possible explanations for this delay, both based on the known segregation of Ag to the surface of Ag-Au alloys (*25*). Unfortunately, we cannot unambiguously discriminate between the two at this point. The first scenario hypothesizes the existence of a low-coverage Ag overlayer (*27*), similar to the UPD layer that Ag forms on Au (111) at potentials positive of the bulk Ag deposition. Dissolution of this conformal layer gives the current peak observed during scans to positive potentials but does not alter the morphology of the sample at the resolution of our images. After the removal of this overlayer, Ag atoms dissolve from terrace sites of the alloy at a much slower rate, resulting in the slow roughening observed on the surface (*28*). In the second scenario, the outer layer of the Ag-Au alloy is not pure Ag but is simply Ag-enriched relative to the bulk (*25*), and the current peak corresponds mainly to the dissolution of Ag atoms from terrace sites in the surface. The resulting vacancies and small vacancy clusters are hypothesized to have low enough mobilities that it takes many minutes for them to fuse into sufficiently large clusters to be seen with our STM.

Our observations suggest that random walk processes responsible for vacancy cluster motion may be biased, owing to vacancy cluster interactions and interactions between vacancy clusters and terrace ledges. Long-range interactions should result from the stress or displacement fields associated with such surface defects. Sieradzki *et al.* (*29*)

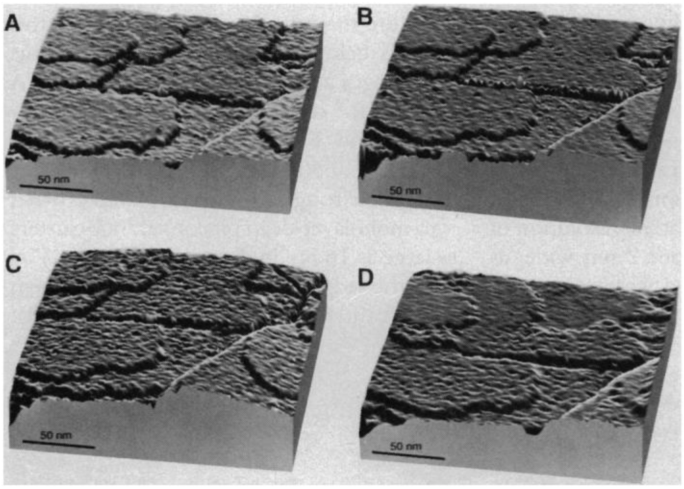

Fig. 2. A time sequence of in situ STM images of a $Ag_{0.04}Au_{0.96}$ alloy sample at (**A**) +0.32 V, (**B**) after 10 min at +0.60 V, (**C**) immediately after increasing the potential to +0.70 V, and (**D**) after 24 min at +0.70 V. Vertical scale ×10.

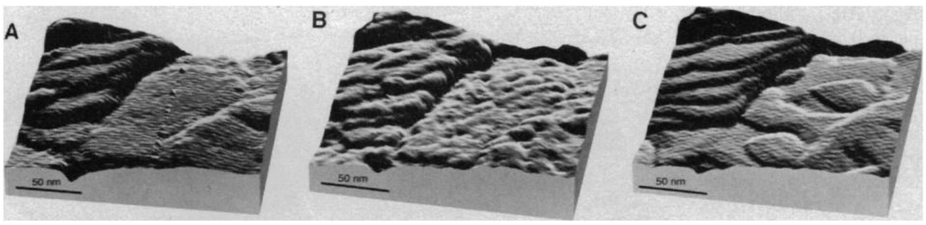

Fig. 3. A time sequence of in situ STM images of a $Ag_{0.15}Au_{0.85}$ alloy sample at (**A**) 0.2 V, and (**B**) 2 min and (**C**) 42 min after reaching +0.70 V and disconnecting the counter electrode. Vertical scale ×10.

have been investigating these issues through computer simulation by using realistic interatomic potentials that model Au (111) surfaces. Their results provide some evidence that interaction effects may be important in the annealing of the roughening resulting from dissolution. For example, they find that as a result of stress field interactions, vacancies are attracted to a down ledge and repelled from an up ledge.

REFERENCES AND NOTES

1. Q. Song, R. C. Newman, R. A. Cottis, K. Sieradzki, *J. Electrochem. Soc.* **137**, 435 (1990).
2. D. E. Williams, R. C. Newman, Q. Song, R. G. Kelly, *Nature* **350**, 216 (1991).
3. K. Sieradzki and R. C. Newman, *Philos. Mag. A* **51**, 95 (1985).
4. H. W. Pickering and C. Wagner, *J. Electrochem. Soc.* **114**, 698 (1967).
5. A. J. Forty and G. Rowlands, *Philos. Mag. A* **43**, 171 (1981).
6. K. Sieradzki, R. R. Corderman, K. Shukla, R. C. Newman, *ibid.* **59**, 713 (1989).
7. R. Sonnenfeld and P. K. Hansma, *Science* **232**, 211 (1986); H. Y. Liu, F. R. F. Fan, C. W. Lin, A. J. Bard, *J. Am. Chem. Soc.* **108**, 3838 (1986).
8. J. Wiechers, T. Twomey, D. M. Kolb, R. J. Behm, *J. Electroanal. Chem.* **248**, 451 (1988).
9. D. J. Trevor, C. E. D. Chidsey, D. N. Loiacono, *Phys. Rev. Lett.* **62**, 929 (1989).
10. D. J. Trevor and C. E. D. Chidsey, *J. Vac. Sci. Technol. B* **9**, 964 (1991).
11. M. P. Green *et al.*, *J. Phys. Chem.* **93**, 2181 (1989).
12. O. M. Magnussen, J. Hotlos, R. J. Nichols, D. M. Kolb, R. J. Behm, *Phys. Rev. Lett.* **64**, 2929 (1990).
13. S. L. Yau, C. M. Vitus, B. C. Schardt, *J. Am. Chem. Soc.* **112**, 3677 (1990).
14. S. Manne, P. K. Hansma, J. Massie, V. B. Elings, A. A. Gewirth, *Science* **251**, 183 (1991).
15. For reviews, see R. Sonnenfeld, J. Schneir, and P. K. Hansma [in *Modern Aspects of Electrochemistry*, R. E. White, J. O. M. Bockris, B. E. Conway, Eds. (Plenum, New York, 1990), vol. 21, pp. 1–28] and C. E. D. Chidsey [in *Applications of Surface Analysis Methods to Environmental/Material Interactions*, D. R. Barv, C. R. Clayton, G. D. Davis, Eds. (Electrochemical Society, Pennington, NJ, 1991), PV 91-7, p. 25].
16. Freshly cleaved mica substrates were thermally bonded with In to a heated Mo plate that was held at 300°C. Ag was evaporated from a resistively heated crucible, and Au was evaporated with an electron beam. The total deposition rates were typically a few angstroms per second. The system pressure was of the order of 5×10^{-7} torr during evaporation. For details of the deposition apparatus, see C. E. D. Chidsey, D. N. Loiacono, T. Sleator, and S. Nakahara [*Surf. Sci.* **200**, 45 (1988)].
17. We determined the Ag content by using elemental standards with the program Fundamental Parameters (Tracor X-ray, Princeton, NJ). This method was confirmed by Rutherford backscattering spectroscopy on the $Ag_{0.15}Au_{0.85}$ sample.
18. The steady-state electrochemical current at the tips was 100 pA or less at the potentials used during the experiments.
19. W. J. Kaiser and R. C. Jaklevic, *Surf. Sci.* **182**, L227 (1987).
20. G. Binnig, H. Rohrer, Ch. Gerber, E. Weibel, *ibid.* **131**, L379 (1983).
21. The small hillocks in Fig. 1A are occasionally observed on Au and Ag-Au alloy samples in air and electrolytes and are not understood.
22. In the experiments with the $Ag_{0.04}Au_{0.96}$ and $Ag_{0.15}Au_{0.85}$ alloys the electrolyte contained 1 mM $AgClO_4$, and the reference electrode was a Ag wire.
23. In the experiments with the $Ag_{0.15}Au_{0.85}$ alloy the electrochemical potential was raised to 0.70 V, at which time the counter electrode was opened and STM images were acquired. The potential of the sample slowly decreased.
24. Although monolayer de-alloying had not been examined before our investigation, polarization curve measurements reported by R. P. Tischer and H. Gerischer [*Z. Elektrochem.* **62**, 50 (1962)] on a series of Ag-Au alloys provide evidence of the compositional dependence of Ag dissolution. Their results indicate that for alloys with less than about 50% by atom Ag, dissolution occurs at potentials close to the Au oxidation potential, whereas for alloys with greater than 50% by atom Ag, dissolution occurs at potentials closer to the potential at which Ag dissolves from a pure Ag electrode.
25. K. Meinel, M. Klaua, H. Bethge, *Phys. Status Solidi A* **106**, 133 (1988); G. A. Somorjai, in *Chemistry and Physics of Solid Surfaces V*, vol. 35 in the *Springer Series in Chemical Physics*, R. Vanselow and R. Howe, Eds. (Springer-Verlag, Berlin, 1984), pp. 1–22.
26. The 2-D percolation threshold for the triangular lattice including first and second near neighbors is 0.295 [V. K. S. Shante and S. Kirpatrick, *Adv. Phys.* **20**, 325 (1971)].
27. Although there is no direct evidence for the formation of a Ag overlayer resulting from segregation in Ag-Au, low-energy ion scattering has shown that segregation of Au to Ni (111) surfaces results in the formation of a pure Au overlayer [T. M. Buck, in *Chemistry and Physics of Solid Surfaces IV*, vol. 20 of the *Springer Series in Chemical Physics*, R. Vanselow and R. Howe, Eds. (Springer-Verlag, Berlin, 1982), pp. 435–464].
28. Once a vacancy or a vacancy cluster is formed, its diffusion in the terrace could determine the rate at which other nearby Ag atoms dissolve, because a Ag atom adjacent to a vacancy probably dissolves more quickly than one isolated in a terrace.
29. K. Sieradzki, F. H. Strietz, I. C. Oppenheim, unpublished results.
30. The work of K.S. and I.C.O. was supported by the U.S. Department of Energy Office of Basic Energy Sciences (contract DE-FG02-90ER45421) and the NSF (contract DMR-9011047).

3 May 1991; accepted 23 July 1991

Early Cambrian Foraminifera from West Africa

STEPHEN J. CULVER

Agglutinated foraminifera have been recovered from siltstones in the Walidiala Valley, Taoudeni Basin, West Africa. Associated faunas suggest an Early Cambrian age for these strata. These now earliest known unequivocal foraminifera help constrain hypotheses concerning the origin of skeletalization at the beginning of the Phanerozoic.

DISCUSSIONS CONCERNING THE APpearance of skeletonization near the base of the Cambrian [about 550 Ma (million years ago)] (*1*) are often restricted to metazoans and take little account of the acquisition of hard parts by protists at the same time. For example, hypotheses relating the evolution of skeletonization to increases in body size (*2*) and to detoxification of excess calcium (*3*) in metazoans do not apply to protists and hence are weakened by the appearance of testate protists in the Early Cambrian (*4*). However, this appearance is not inconsistent with the hypothesis, applicable to both metazoans and protists, that the initial function of skeletons was to protect the organism, primarily against predation (*5*). The presence of agglutinated foraminifera in the Lower Cambrian, probably Atdabanian Stage–equivalent strata, of the Taoudeni Basin, West Africa, is reported here. These specimens extend considerably the known geologic range of several genera, they represent the earliest known unequivocal foraminifera, and they further remind us that protists as well as metazoans should be considered in accounting for the origin of skeletalization.

The unmetamorphosed and generally undeformed Taoudeni Basin strata have been divided into three supergroups (*6*). Supergroup 1 is entirely Proterozoic in age, Supergroup 2 (about 1200 m thick) commences with an Upper Proterozoic tillite, and Supergroup 3 commences with an Upper Ordovician tillite (*6*). In the Walidiala valley at the Senegal-Guinea border, only the lower portion of Supergroup 2 is present and is represented by the Mali group (Fig. 1). This has been divided into the Hassanah Diallo Formation, composed of glacial diamictites and laminated siltstones with ice-rafted dropstones and representing the Late Proterozoic (Vendian) glaciation of West Africa (*6–11*), and the overlying Nandoumari Formation, commencing with intermittent quartz arenites (Tanague Member), and overlain by dolomites (Bowal Member) and green and red siltstones (Fougon Member) (*8*). The dolomites are of supratidal to shallow subtidal origin. Subtidal dolomites are interbedded with siltstones that pass conformably into the overlying Fougon Member siltstones. Hence, the Fougon Member is also of probable shallow marine origin (*8*).

A few specimens of small shelly fossils have been recovered from Bowal Member dolomites (*7*) and several hundred additional small shelly fossils and several agglutinated foraminifera have been recovered from two samples of the immediately overlying siltstones of the Fougon Member (Fig. 2).

Supergroup 2 strata in the Taoudeni Basin are poorly fossiliferous. The only recorded macrofossils from Supergroup 2 are inarticulate brachipods from near the top of the unit in the Mauritanian Adrar which indi-

---

Department of Geological Sciences, Old Dominion University, Norfolk, VA 23529.